SARS-CoV-2 ORF3a inhibits cGAS-STING-mediated autophagy flux and antiviral function

Jiaming Su[1,2,5] , Si Shen[1,5] , Ying Hu[1,5] , Shiqi Chen[1] , Leyi Cheng[1] , Yong Cai[3] , Wei Wei[4], Yanpu Wang[1,2,*] , Yajuan Rui[1,2,*] , Xiao-Fang Yu[1,2,*]

[1]Cancer Institute (Key Laboratory of Cancer Prevention and Intervention, China National Ministry of Education), The Second Affiliated Hospital, Zhejiang University School of Medicine, Hangzhou, Zhejiang, China.

[2]Cancer Center, Zhejiang University, Hangzhou, Zhejiang, China.

[3]School of Life Science, Jilin University, Changchun, China.

[4]Key Laboratory of Organ Regeneration and Transplantation of the Ministry of Education, Institute of Translational Medicine, Institute of Virology and AIDS Research, The First Hospital of Jilin University, Changchun, China.

[5]These authors contributed equally: Jiaming Su, Si Shen, Ying Hu.

*Correspondence: wangyanpu@zju.edu.cn, yrui@zju.edu.cn and xfyu1@zju.edu.cn.

Keywords: SARS coronavirus < Virus classification, Innate immunity < Immune responses, Coronavirus < Virus classification

**Abstract**

Recognizing aberrant cytoplasmic dsDNA and stimulating cGAS-STING-mediated innate immunity are essential for the host defense against viruses. Recent studies have reported that SARS-CoV-2 infection, responsible for the COVID-19 pandemic, triggers cGAS-STING activation. cGAS-STING activation can trigger IRF3-type I interferon (IFN) and autophagy-mediated antiviral activity. Although viral evasion of STING-triggered IFN-mediated antiviral function has been well studied, studies concerning viral evasion of STING-triggered autophagy-mediated antiviral function are scarce. In the present study, we have discovered that SARS-CoV-2 ORF3a is a unique viral protein that can interact with STING and disrupt the STING-LC3 interaction, thus blocking cGAS-STING-induced autophagy but not IRF3-type I IFN induction. This novel function of ORF3a, distinct from targeting autophagosome-lysosome fusion, is a selective inhibition of STING-triggered autophagy to facilitate viral replication. We have also found that activation of bat STING can induce autophagy and antiviral activity despite its defect in IFN induction. Furthermore, ORF3a from bat coronaviruses can block bat STING-triggered autophagy and antiviral function. Interestingly, the ability to inhibit STING-induced autophagy appears to be an acquired function of SARS-CoV-2 ORF3a, since

This article has been accepted for publication and undergone full peer review but has not been through the copyediting, typesetting, pagination and proofreading process, which may lead to differences between this version and the Version of Record. Please cite this article as doi: 10.1002/jmv.28175.

SARS-CoV ORF3a lacks this function. Taken together, these discoveries identify ORF3a as a potential target for intervention against COVID-19.

**Introduction**

The COVID-19 pandemic, caused by severe acute respiratory syndrome coronavirus 2 (SARS-CoV-2), has swept the world since 2019, causing an epic public health crisis and posing a tremendous economic burden[1,2]. To date, the rampant spread of SARS-CoV-2 has caused over 555 million infections and 6.3 million deaths worldwide[3]. Thus, it is urgent that we clearly delineate the pathogenesis of SARS-CoV-2 and identify efficient therapies to antagonize this potentially deadly virus.

The DNA pattern recognition receptor cyclic GMP-AMP synthase (cGAS) is a key sensor for recognizing viral infection in the cytoplasm of cells[4]. Recent studies have demonstrated that SARS-CoV-2 infection disrupts mitochondrial homeostasis, inducing mitochondrial DNA (mtDNA) release[5]. It also causes syncytia formation, which leads to the shuttling of chromatin and micronuclei from the nucleus to the cytoplasm[6,7]. This aberrant cytoplasmic DNA is sensed by cGAS, activating cGAS-STING-mediated antiviral responses. To date, cGAS-STING-mediated, IRF3-type I-interferon (IFN)-dependent antiviral defenses and the counteracting responses by diverse viruses, including SARS-CoV-2, have been widely reported[4,8]. Apparently, STING-mediated type I IFN is dampened in bats, which are often commensal with multiple viruses, including coronaviruses[9]. Bat coronaviruses (CoVs) are highly conserved when compared to SARS-CoV-2 and are believed to be the most likely origin of SARS-CoV-2[10]. These observations have led us to speculate that the type I IFN-independent function of STING may play an important role in antiviral responses.

Autophagy is a fundamental and highly conserved intracellular degradation process in eukaryotes for eliminating damaged organelles, protein aggregates, and invading pathogens[11]. cGAS-STING-induced autophagy is a primordial type I IFN-independent activity that can significantly inhibit the replication of viruses[12], but little is known about how viruses thwart this cGAS-STING-triggered autophagy. We now propose that in order to facilitate its survival, SARS-CoV-2 may have evolved evasion strategies to suppress autophagy.

In the present study, by screening reported STING suppressors and SARS-CoV-2-encoded proteins, we have identified ORF3a as a potent inhibitor of STING-mediated autophagy that facilitates viral replication. In addition, we have found that bat-CoV ORF3a can antagonize bat STING-triggered autophagy, and this suppression can be neutralized by a small molecule inhibitor, TPEN. Notably, among human coronaviruses, only SARS-CoV and SARS-CoV-2 encode ORF3a. We found that, as compared to SARS-CoV-2, SARS-CoV ORF3a is less effective in defending against STING-mediated autophagy, which may explain the epidemic potential of SARS-CoV-2. Taken together, our results indicate the unique role of the SARS-CoV-2 ORF3a in suppressing STING-mediated autophagy, which benefits viral replication and also provides potential targets for the development of therapeutic strategies against SARS-CoV-2.

## Materials and Methods

### Viruses and Cell Lines

HEK293T cells (ATCC, CRL-3216) and HeLa cells (ATCC, CCL-2) were cultured in Dulbecco's modified Eagle's medium (DMEM) supplemented with 10% fetal bovine serum (FBS) and 1% penicillin/streptomycin solution. EV-A71 and HSV-1 GFP were prepared as previously described[13].

### Plasmids, Antibodies and Reagents

mCherry-GFP-LC3 (#22418), mCherry-LC3 (#40827) were purchased from Addgene. *Nematostella vectensis*, *Myotis davidii*, *Rhinolophus sinicus*, *Mus musculus*, *Gallus gallus*, *Xenopus tropicalis*, and *Danio rerio* STING-Flag; HPV E7-HA (NC_001357.1), Adenovirus E1A-HA (NC_001405.1), KHSV vIRF1-HA (NC_009333.1), HCV NS4B-HA (YP_009709868.1), HCMV UL82-HA (P06726.2), YFC NS4B-HA (NP_776008.1), DENV NS2B3-HA (P14340.2), ZC45 ORF3a-HA (MG772933.1), RaTG ORF3a-HA (QHR63301.1) and ORF3a chimeras were obtained from Generay Biotech Co., Ltd, CN, and cloned into VR1012. All the coronavirus protein constructs, *Homo sapiens* STING wild-type and truncation plasmids, Myc-cGAS, IFNα, and NF-κB luciferase reporter plasmids and Vpx-HA have been described previously[14,15]. Plasmids were verified by sequencing before transfection using the Hieff TransTM Liposomal Transfection Reagent (YeasenBiotech, CN) according to the manufacturer's instructions.

The following antibodies were used for Western blotting or immunofluorescence: anti-Flag (Sigma, F3165), anti-Myc (Millipore, 05-724), anti-p62 (MBL, PM045), anti-LC3B (Sigma, L7543), anti-GAPDH (Proteintech, 60004-1-Ig), anti-HA (Invitrogen, 71-5500), anti-Histone (Genscript, A01502), anti-IFIT3 (Proteintech, 15201-1-AP), anti-IRF3-p (Cell Signal, 4974), GM130 (abcam, ab52649), DAPI (Sigma, 28718-90-3), bafilomycin A1 (MCE, HY-100558), anti-Flag M2 Affinity Gel (Sigma, A2220), Alexa Fluor 488 AffiniPure Goat Anti-Mouse IgG (H+L) (Yeasen, 33106ES60) and Alexa Fluor 647 AffiniPure Goat Anti-Rabbit IgG (H+L) (Yeasen, 33113ES60). HRP-conjugated secondary antibodies (anti-mouse or anti-rabbit) were purchased from HuaBio.

### Virus Infection and Quantitation

HEK293T cells were transfected with indicated plasmids and then infected with HSV-1 GFP and EV-A71. At 24 h post-infection, the cells were washed with cold PBS, and HSV-1 GFP was measured by flow cytometry according to the manufacturer's instructions. EV-A71-infected cells were observed for morphological changes and photographed by light microscopy at 100× magnification. The viral RNA levels of EV-A71 were evaluated by real-time PCR using SYBR Green. EV-A71-VP1 primers: Forward, 5'- CAAGGGATGGTACTGGAAGT-3'; Reverse, 5'-GATCGGTAGAGGTAGTGGAA-3'.

### Dual-luciferase Assays

HEK293T cells were transfected with 100 ng of the *Firefly luciferase* reporter plasmids for the IFNα promoter and NF-κB response element; 5 ng of *Renilla luciferase* control plasmid (pRL-TK); and the indicated amounts of the expression plasmids per well. Dual-luciferase activity were measured as previously described[14].

**Confocal Microscopy**

HeLa cells were transfected with the indicated plasmids, with or without bafilomycin-A1. Images were captured as previously described[14].

**Flow Cytometry**

After HSV-1 GFP infection, cells were washed with cold PBS and analyzed on a DxFLEX flow cytometer (Beckman Coulter). Apoptosis was evaluated using an Annexin V-APC/7AAD apoptosis kit (Multi Sciences Biotech, CN). A DxFLEX flow cytometer (Beckman Coulter) was used to quantify apoptosis detection, and all the data analysis was performed using FlowJo software.

**Co-immunoprecipitation (Co-IP)**

HEK293T cells were seeded into 6-cm dishes and transfected with the indicated plasmids using Hieff TransTM Liposomal Transfection Reagent (YeasenBiotech, China), with or without bafilomycin-A1. Immunoblotting and co-immunoprecipitation were performed as previously described[14].

**Immunoblot Band Quantitation**

Quantification of band intensities was performed using ImageJ (version 1.50i).

**Statistical Analysis**

Data analyses were performed using GraphPad Prism 6.0 software. All data are shown as means ± SD. The statistical significance analyses were performed using a two-sided unpaired *t*-test (P values) with exact values.

**Results**

To investigate the involvement of the cGAS-STING signaling pathway across phylogenetic kingdoms in innate immune activation and antiviral defense, we employed diverse STING molecules from *Homo sapiens* to *Nematostella vectensis* (Fig. 1a). Using established experimental systems for the detection of cGAS-STING-triggered innate immune activation, we discovered that different STING molecules exhibited different activity in terms of stimulating downstream IFNα and NF-κB responses (Fig. 1b). For these experiments, the replication of herpes simplex virus (HSV) was evaluated in HEK293T cells. As compared to *Homo sapiens* STING (*Hsa*STING), STING in the bats *Rhinolophus sinicus* and *Myotis davidii* (*Rss*STING and *Myd*STING) was defective in the induction of type I IFN, as has been previously reported[9]; however, these STING molecules restricted HSV-1 replication efficiently, indicating the presence of a cGAS-STING-signaling antiviral defense acting in a type I IFN-independent fashion (Fig. 1c, d). In addition, STING from *Xenopus tropicalis* and *Nematostella vectensis* (*Xtr*STING and *Nve*STING), which barely induced activation of the NF-κB response element, also showed a significant inhibition of HSV-1 replication, suggesting that the cGAS-STING antiviral defense is independent of NF-κB induction. A unique and important feature of the cGAS–STING pathway is the robust activation of autophagy in addition to the induction of interferons and NF-κB responses[12]. We observed that overexpression of cGAS-STING induced the activation of autophagic flux, as monitored by p62 degradation and LC3 lipidation (Fig.

1e, f). Notably, STING from all the various species examined was capable of triggering autophagy induction (Fig. 1e, f) and efficiently restricted HSV-1 replication (Fig. 1c, d). Thus, the cGAS-STING-triggered antiviral defense appeared to be independent of IFN and NF-κB signaling. Moreover, the induction-related autophagy of cGAS-STING appeared to be an evolutionarily conserved activity that played a dominant role in antagonizing viral replication.

All viruses have developed efficient evasion mechanisms in order to survive. In previous studies we have demonstrated that SARS-CoV-2 proteins are capable of a unique and complementary suppression of cGAS-STING and RNA sensing-triggered innate immune responses[14]. Since cGAS-STING-triggered autophagy is prominent in antiviral replication[12], we conducted screening to determine whether any viral proteins could potentially target the STING-autophagy axis. For this purpose, we synthesized viral proteins from RNA viruses (SARS-CoV-2 ORF3a, HCV NS4B, DENV NS2B3 and YFV NS4B), DNA viruses (HPV E7, HCMV UL82, AdV E1A and KHSV vIRF1), and retrovirus (HIV-2/SIV Vpx) that have been reported to associate with STING and subsequently disrupt STING's downstream signalosome assembly. To further exclude the effect of STING-mediated interferon activity against DNA viruses, we generated a construct with a STING C-terminal tail truncation (STING dCTT) that is defective in the stimulation of type I IFN and type I IFN-stimulated gene expression[15] but functional in terms of autophagy induction[12] (Fig. 2a). Surprisingly, the SARS-CoV-2 ORF3a could be distinguished from various other viral proteins in terms of impeding cGAS-STING-mediated p62 degradation, as shown in Fig. 2b, c. It has been reported that SARS-CoV-2 3CL can also inhibit cGAS-STING signaling[14]. Therefore, we asked whether other SARS-CoV-2 structural and accessory proteins (Fig. 2d) might be involved in STING-based suppression of autophagy induction. For this purpose, we co-expressed cGAS-STING dCTT with each individual SARS-CoV-2 viral protein in HEK293T cells and discovered that only ORF3a significantly restored p62 expression (Fig. 2e, f). We observed an interaction of ORF3a with STING as well as STING dCTT, both of which are competent to induce autophagy (Fig. S1a, Fig. 2a). Moreover, we detected intracellular co-localization of STING and ORF3a (Fig. S1b). STING activation induces co-localization of STING and LC3 which is important for STING-triggered autophagy[16]. We discovered that ORF3a inhibited the co-localization of STING and LC3 (Fig. 2g). Consistent with this observation, we also discovered that ORF3a inhibited the interaction between STING and LC3-II (Fig. S2a).

Furthermore, ORF3a efficiently restored the replication of HSV-1 (Fig. 2h-j) and EV-A71 (Fig. S3a, b), which had been repressed in the presence of cGAS-STING dCTT. We have previously demonstrated that SARS-CoV-2 ORF3a selectively inhibits cGAS-STING-NF-κB signaling, but not the RIG-I-like Receptor (RLR) pathway[14], implying that the cGAS-STING pathway is a crucial barrier during SARS-CoV-2 infection and that SARS-CoV-2 ORF3a is a potent inhibitor of cGAS-STING. In addition, the SARS-CoV-2 ORF3a has a Cys-rich region with the potential to bind zinc. Interestingly, we found that N, N, N′, N′-tetrakis (2-pyridylmethyl)-ethylenediamine (TPEN), a lipid-soluble zinc metal chelator, was able to block ORF3a function (Fig. S2b). Taken together, these data indicate that, among diverse viral proteins,

SARS-CoV-2 ORF3a is a unique and potent inhibitor of the STING-autophagy axis that facilitates efficient viral replication and helps viral pathogenesis.

Bats serve as reservoirs for many viruses, including coronaviruses[9]. STING molecules in all the bats examined to date have proved defective for the induction of type I IFN and have compromised antiviral activity. We have now demonstrated that STING from the bats *Rhinolophus sinicus* (*Rss*STING) and *Myotis davidii* (*Myd*STING)[9] can induce autophagy (Fig. 1e, f). Interestingly, though, diverse ORF3a molecules encoded by bat coronaviruses (Fig. 3a) have evolved an evolutionarily conserved suppression of bat STING dCTT-triggered autophagy (Fig. 3b-d). Functionally, bat ORF3as, including *RaTG* and *ZC45*, were effective in rescuing HSV-1 suppression induced by *Rss*STING dCTT-mediated autophagy induction (Fig. 3e, f).

Since, ORF3a is only encoded by SARS-CoV and SARS-CoV-2 among human coronaviruses, and this ORF is conserved in terms of the induction of apoptosis (Fig. 4a-c) and antagonism of cGAS-STING-mediated NF-κB activity (Fig. 4d), we wondered whether SARS-CoV and SARS-CoV-2 ORF3a would both be able to suppress STING-mediated autophagy. Surprisingly, we discovered that the ORF3a derived from SARS-CoV was less capable of inhibiting STING-triggered p62 degradation (Fig. 4e, f), and autolysosome formation (Fig. S4a, b) than was SARS-CoV-2 ORF3a. To pursue this question further, we constructed an ORF3a S2-S1 chimera that consisted of the N-terminus of SARS-CoV-2 ORF3a and the C-terminus of SARS-CoV ORF3a, and this chimera showed a loss of function (Fig. 4g, h). Interestingly, the ORF3a S1-S2 chimera, unlike SARS-CoV-2 ORF3a[17,18], lost the ability to inhibit the fusion of autophagosomes with lysosomes (Fig. 4g, Fig. S4c, d) but maintained the ability to inhibit STING–triggered autophagy (Fig. S4e, f). Consistently, SARS-CoV-2 ORF3a and the S1-S2 chimera showed stronger neutralization of cGAS-STING dCTT autophagy-mediated HSV-1 inhibition than did SARS-CoV ORF3a or the chimeric ORF3a S2-S1 (Fig. 4i-l, Fig. S4g, h). This unusual effect of the SARS-CoV-2 ORF3a may have contributed to some of the unique biological properties of the SARS-CoV-2.

**Discussion**

Evasion of host innate immunity is essential for the survival of viruses. We have shown that SARS-CoV-2 infection triggers cGAS-STING activation, which leads to the generation of type I IFN and autophagy-mediated antiviral activity. The means by which viruses evade cGAS-STING-triggered, autophagy-mediated antiviral activity is poorly understood[19]. ORF3a is a virion-associated protein[20], and thus it plays an important role in the early stage of SARS-CoV-2 infection. We observed here that SARS-CoV-2 ORF3a was able to block cGAS-STING-induced autophagy and its antiviral activity (Fig. 2b-j). Surprisingly, SARS-CoV ORF3a had an impaired ability to block cGAS-STING-induced autophagy and the resulting antiviral activity (Fig. 4e-l), although ORF3a from both SARS-CoV and SARS-CoV-2 maintained the ability to induce apoptosis (Fig. 4a-c)[21] and NF-κB inhibition (Fig. 4d)[14].

SARS-CoV-2 ORF10 has also been reported to inhibit cGAS-STING-induced autophagy[8]. Unlike ORF10, which also affects STING foci formation and IRF3

activation, ORF3a specifically affects cGAS-STING-induced autophagy, without affecting STING foci formation or IRF3 activation (Fig. 4m).

Bat STING is defective in stimulating IRF3-type I IFN activation (Fig. 1b)[9]; however, we have now discovered that bat STING activation can still induce autophagy and antiviral activity (Fig. 1c-f). On the other hand, ORF3a from bat coronavirus has the ability to suppress bat STING-triggered autophagy and its antiviral function (Fig. 3b-f), even though STING-mediated autophagy is a primordial, conserved antiviral activity[12]. The ability to inhibit STING-induced autophagy appears to be an acquired attribute of SARS-CoV-2 and bat coronavirus ORF3a, and this inhibition is sensitive to a small-molecule inhibitor, namely TPEN (Fig. S2b). Thus, our study identifies ORF3a as a potential drug target for intervention against COVID-19.

**Acknowledgments**

This work was supported in part by funding from the National Natural Science Foundation of China (numbers 82102384, 82172239, 92169203, 31900133, 31970151, 32041006), National Natural Science Foundation of Zhejiang Province (LY22C080002, LQ21C010001), and Leading Innovative and Entrepreneur Team Introduction Program of Zhejiang (2019R01007). We thank Q. Dong for helping with the confocal microscopy analysis and N. Zhao, Y. Huang and Q. Lv for providing technical assistance.

**Conflict of Interests**

The authors declare no competing interests.

**Author Contributions**

J.S., S.S. and Y.H. carried out most of the biochemical experiments, with help from Y.W., S.C. and L.C.. Y.W. conducted the immunostaining and confocal microscopy experiments. Y.C. and W. W. contributed the key reagents. J.S., S.S. and Y.R. performed the viral infection experiments and plasmid construction. X.-F.Y., Y.R. and Y.W contributed to the supervision and data analysis. X.-F.Y. directed the project, analysed the data and wrote the paper, with help from all of the authors.

**Data Availability Statement**

All data, materials, and methods are included in the article.

**ORCID**

Xiao-Fang Yu https://orcid.org/0000-0002-6104-3456

**References**

1 Berlin, D. A., Gulick, R. M. & Martinez, F. J. Severe Covid-19. *N Engl J Med* **383**, 2451-2460, doi:10.1056/NEJMcp2009575 (2020).

2 Zhu, N. *et al.* A Novel Coronavirus from Patients with Pneumonia in China, 2019. *The New England journal of medicine* **382**, 727-733, doi:10.1056/NEJMoa2001017 (2020).

3 Dong, E., Du, H. & Gardner, L. An interactive web-based dashboard to track

COVID-19 in real time. *Lancet Infect Dis* **20**, 533-534, doi:10.1016/s1473-3099(20)30120-1 (2020).

4 Ma, Z. & Damania, B. The cGAS-STING Defense Pathway and Its Counteraction by Viruses. *Cell host & microbe* **19**, 150-158, doi:10.1016/j.chom.2016.01.010 (2016).

5 Domizio, J. D. *et al.* The cGAS-STING pathway drives type I IFN immunopathology in COVID-19. *Nature* **603**, 145-151, doi:10.1038/s41586-022-04421-w (2022).

6 Zhou, Z. *et al.* Sensing of cytoplasmic chromatin by cGAS activates innate immune response in SARS-CoV-2 infection. *Signal Transduct Target Ther* **6**, 382, doi:10.1038/s41392-021-00800-3 (2021).

7 Liu, X. *et al.* SARS-CoV-2 spike protein-induced cell fusion activates the cGAS-STING pathway and the interferon response. *Sci Signal* **15**, eabg8744, doi:10.1126/scisignal.abg8744 (2022).

8 Han, L. *et al.* SARS-CoV-2 ORF10 antagonizes STING-dependent interferon activation and autophagy. *J Med Virol*, doi:10.1002/jmv.27965 (2022).

9 Xie, J. *et al.* Dampened STING-Dependent Interferon Activation in Bats. *Cell Host Microbe* **23**, 297-301.e294, doi:10.1016/j.chom.2018.01.006 (2018).

10 Ruiz-Aravena, M. *et al.* Ecology, evolution and spillover of coronaviruses from bats. *Nat Rev Microbiol* **20**, 299-314, doi:10.1038/s41579-021-00652-2 (2022).

11 Deretic, V., Saitoh, T. & Akira, S. Autophagy in infection, inflammation and immunity. *Nat Rev Immunol* **13**, 722-737, doi:10.1038/nri3532 (2013).

12 Gui, X. *et al.* Autophagy induction via STING trafficking is a primordial function of the cGAS pathway. *Nature* **567**, 262-266, doi:10.1038/s41586-019-1006-9 (2019).

13 Rui, Y. *et al.* Disruption of MDA5-Mediated Innate Immune Responses by the 3C Proteins of Coxsackievirus A16, Coxsackievirus A6, and Enterovirus D68. *J Virol* **91**, doi:10.1128/jvi.00546-17 (2017).

14 Rui, Y. *et al.* Unique and complementary suppression of cGAS-STING and RNA sensing- triggered innate immune responses by SARS-CoV-2 proteins. *Signal Transduction and Targeted Therapy* **6**, 123, doi:10.1038/s41392-021-00515-5 (2021).

15 Su, J. *et al.* HIV-2/SIV Vpx targets a novel functional domain of STING to selectively inhibit cGAS–STING-mediated NF-κB signalling. *Nature Microbiology* **4**, 2552-2564, doi:10.1038/s41564-019-0585-4 (2019).

16 Liu, D. *et al.* STING directly activates autophagy to tune the innate immune response. *Cell Death Differ* **26**, 1735-1749, doi:10.1038/s41418-018-0251-z (2019).

17 Zhang, Y. *et al.* The SARS-CoV-2 protein ORF3a inhibits fusion of autophagosomes with lysosomes. *Cell Discov* **7**, 31, doi:10.1038/s41421-021-00268-z (2021).

18 Miao, G. *et al.* ORF3a of the COVID-19 virus SARS-CoV-2 blocks HOPS complex-mediated assembly of the SNARE complex required for autolysosome formation. *Developmental cell* **56**, 427-442.e425, doi:10.1016/j.devcel.2020.12.010 (2021).

19 Zhang, R., Kang, R. & Tang, D. The STING1 network regulates autophagy and cell death. *Signal Transduction and Targeted Therapy* **6**, 208, doi:10.1038/s41392-021-00613-4 (2021).

20 Shen, S. *et al.* The severe acute respiratory syndrome coronavirus 3a is a novel structural protein. *Biochem Biophys Res Commun* **330**, 286-292, doi:10.1016/j.bbrc.2005.02.153 (2005).

21 Ren, Y. *et al.* The ORF3a protein of SARS-CoV-2 induces apoptosis in cells. *Cell Mol Immunol* **17**, 881-883, doi:10.1038/s41423-020-0485-9 (2020).

**Figure legends**

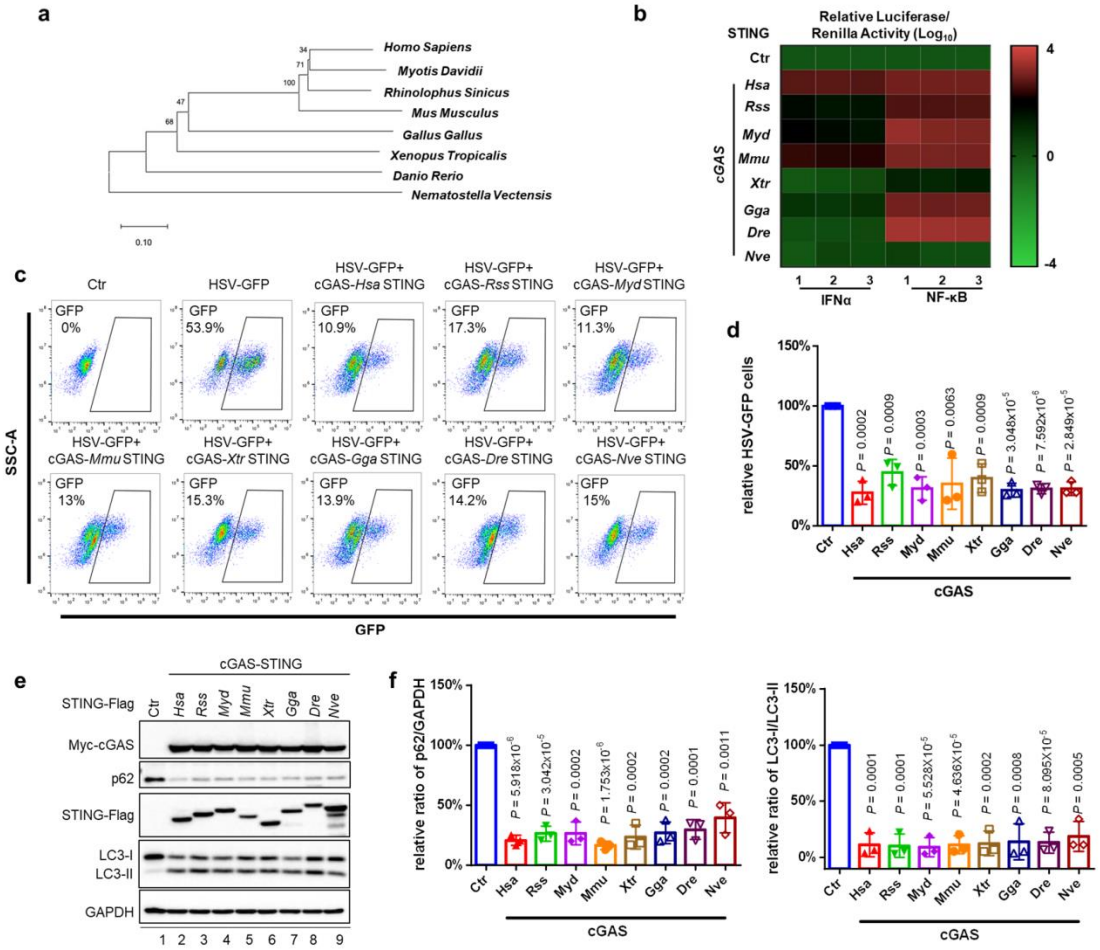


**Fig. 1 Activation of STING from diverse species is evolutionarily conserved in terms of autophagy induction and antagonizes virus replication efficiently.**
**a. Phylogenetic tree of STING from vertebrates and *Nematostella vectensis***

**(*Nve*STING).** Reference sequences of representative STING molecules include *Homo sapiens* (*Hsa*, NP_938023.1), *Myotis davidii* (*Myd*, XP_006772500.1), *Rhinolophus sinicus* (*Rss*, XP_019595754.1), *Mus musculus* (*Mmu*, NP_082537.1), *Gallus gallu*s (*Gga*, NP_001292081.1), *Xenopus tropicalis* (*Xtr*, NP_001106445.2), *Danio reri*o (*Dre*, NP_001265766.1), and *Nematostella vectensis* (*Nve*, XP_001627385.1) STING. Phylogenetic analysis was performed with the MEGA X program by the neighbor-joining method on the basis of the Kimura two-parameter model.

**b. Activation of the various STING molecules varies in terms of downstream responses.** HEK293T cells were transfected with IFNα-Luc or NF-κB-Luc, together with Myc-cGAS and various STING expression vectors. pRL-TK *Renilla* was used as an internal control. Transactivation of the luciferase reporter was determined 24 h after transfection. Results are shown for n = 3 independent experiments.

**c-d. Activation of vertebrate STING and *Nve*STING inhibits HSV-1 GFP replication.** HEK293T cells were co-transfected with Myc-cGAS and various STING expression vectors for 20 h, then infected with HSV-1 GFP for 24 h. GFP-positive cells were analyzed by FACS(**c**). The relative HSV-1 GFP positivity is shown in (**d**). Empty vector with HSV-1 GFP infection served as a control and was set to 100%. Statistical significance was determined by two-sided unpaired *t*-test. Means and standard deviations are presented. Results are shown for n = 3 independent experiments.

**e-f. Autophagy induction triggered by the cGAS-STING pathway is evolutionarily conserved.** HEK293T cells were co-transfected with Myc-cGAS and various STING expression vectors. Cells were harvested 24 h after transfection. The indicated proteins were analyzed by immunoblotting with anti-p62, anti-LC3, anti-Myc, anti-Flag, and anti-GAPDH, respectively (**e**). Relative p62 and LC3-I/LC3-II levels in (**e**) were quantified with ImageJ software (**f**). Empty vector alone served as a control and was set to 100%. Statistical significance was determined by two-sided unpaired *t*-test. Means and standard deviations are presented. Results are shown for n = 3 independent experiments (representative immunoblotting results are shown).

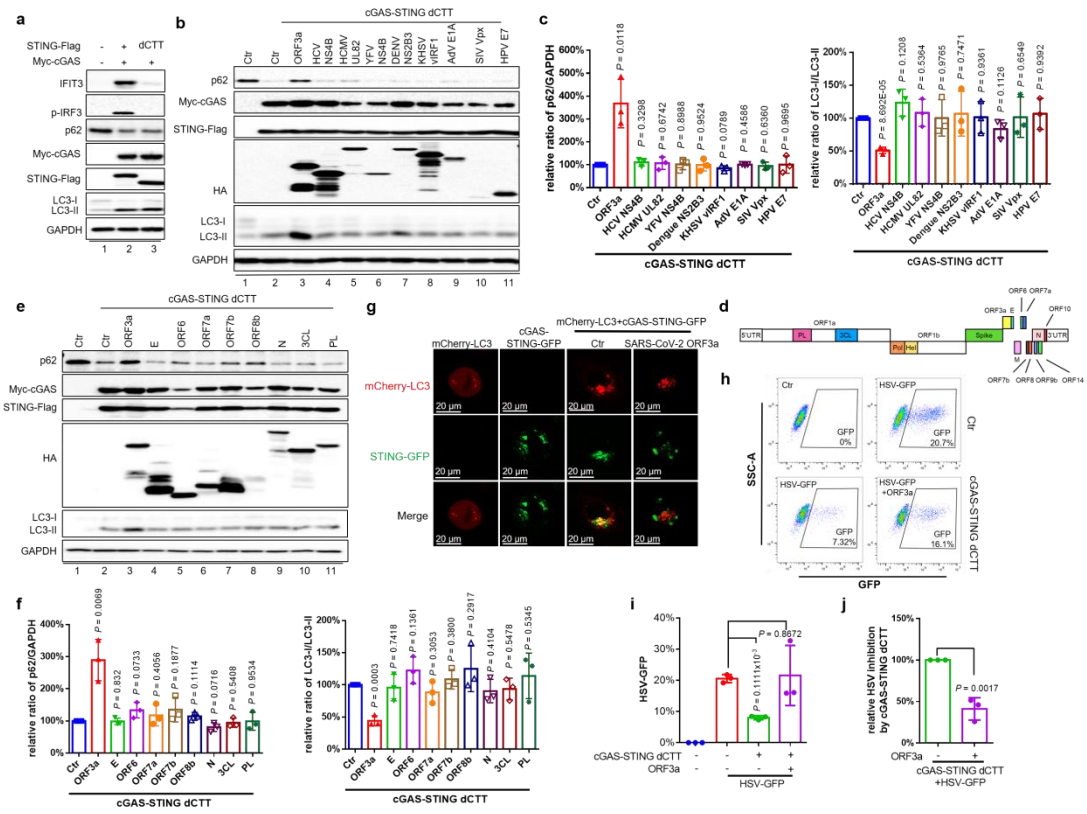

**Fig. 2 SARS-CoV-2 ORF3a is a potent and unique inhibitor of STING-mediated autophagy among viral proteins from RNA viruses, DNA viruses, and retrovirus.**
**a. STING-dCTT can induce autophagy despite its inability to activate the IRF3 pathway.** HEK293T cells were transfected with Myc-cGAS and STING-Flag or STING dCTT-Flag for 24 h. The cells were harvested, and the indicated proteins were analyzed by immunoblotting with anti-IFIT3, anti-p-IRF3, anti-p62, anti-LC3, anti-Myc, anti-Flag, and anti-GAPDH. Results are shown for n = 3 independent experiments (representative immunoblotting results are shown).
**b-c. Among other viral proteins reported to cause cGAS-STING signaling inhibition, only SARS-CoV-2 ORF3a antagonizes cGAS-STING dCTT-induced autophagy.** HEK293T cells were transfected with Myc-cGAS and STING dCTT-Flag expression vectors in the presence or absence of vectors expressing viral proteins as indicated. Cells were harvested 24 h after transfection. The indicated proteins were analyzed by immunoblotting with anti-p62, anti-LC3, anti-Myc, anti-Flag, anti-HA, and anti-GAPDH (**b**). Relative p62 and LC3-I/LC3-II levels in (**b**) were quantified with ImageJ software (**c**). cGAS-STING dCTT alone served as a control and was set to 100%. Statistical significance was determined by two-sided unpaired *t*-test. Means and standard deviations are presented. Results are shown for n = 3 independent experiments (representative immunoblotting results are shown).
**d. Schematic diagram of the genomic organization and encoded proteins of SARS-CoV-2 from the 2019 Wuhan-Hu-1 strain (MN908947.3).**
**e-f. ORF3a is the only protein among SARS-CoV-2 encoded proteins to antagonize cGAS-STING dCTT-induced autophagy.** HEK293T cells were co-transfected with the Myc-cGAS and STING dCTT-Flag expression vectors in the

presence or absence of SARS-CoV-2-encoded proteins. Cells were harvested 24 h after transfection. The indicated proteins were analyzed by immunoblotting with anti-p62, anti-LC3, anti-Myc, anti-Flag, anti-HA, and anti-GAPDH(**e**). Relative p62 and LC3-I/LC3-II levels in (**e**) were quantified with ImageJ software (**f**). cGAS-STING dCTT alone served as a control and was set to 100%. Statistical significance was determined by two-sided unpaired *t*-test. Means and standard deviations are presented. Results are shown for n = 3 independent experiments.

**g. SARS-CoV-2 ORF3a disrupts cGAS-STING-LC3 co-localization specifically.** HeLa cells were transfected as shown and treated with bafilomycin-A1 (0.2 μM). After 24 h, the cells were visualized by confocal microscopy. Scale bars, 20 μm. Results are shown for n = 3 independent experiments (representative images are shown).

**h-j. HSV-1 GFP replication suppressed by cGAS-STING dCTT activation is partially restored by SARS-CoV-2 ORF3a.** HEK293T cells were co-transfected with Myc-cGAS and STING dCTT-Flag expressing vectors in the presence or absence of SARS-CoV-2 ORF3a for 20 h and subsequently infected with HSV-1 GFP for 24 h. GFP-positive cells were analyzed by FACS (**h**). The percentage of GFP-positive cells (**i**) and relative HSV-1 GFP inhibition (**j**) are shown. Empty vector served as a control (**i**), and HSV-1 GFP inhibited by cGAS-STING dCTT served as a positive control and was set to 100% (**j**). Statistical significance was determined by two-sided unpaired *t*-test. Means and standard deviations are presented. Results are shown for n = 3 independent experiments.

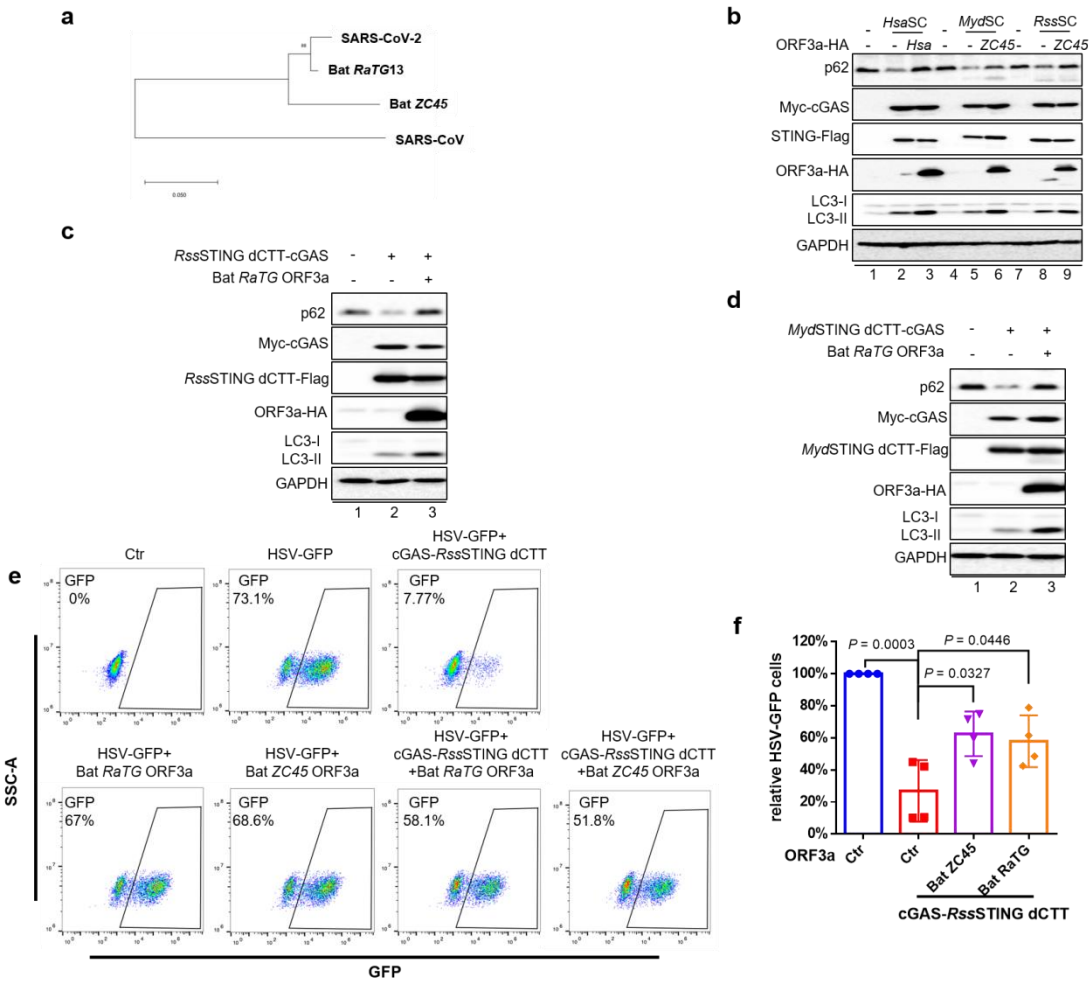


**Fig. 3 Bat-CoV ORF3a can antagonize bat STING-mediated induction of autophagy.**

**a. Phylogenetic tree of ORF3a from SARS-CoV-2, SARS-CoV, and bat-CoVs.** Reference sequences of representative molecules: SARS-CoV-2 (MN908947.3), SARS-CoV (AY278741.1), bat *RaTG13* (QHR63301.1), bat *ZC45* (MG772933.1). Phylogenetic analysis was performed with the MEGA X program by the neighbour-joining method on the basis of the Kimura two-parameter model.

**b. ORF3as from SARS-CoV-2 and bat-CoV antagonize autophagy induction through homologous STING activation.** HEK293T cells were co-transfected with Myc-cGAS and human STING (*Hsa*STING), *Myotis davidii* STING (*Myd*STING), or *Rhinolophus sinicus* STING (*Rss*STING) expression vector in the presence or absence of vectors expressing SARS-CoV-2 ORF3a and bat *ZC45* ORF3a. Cells were harvested 24 h after transfection. The indicated proteins were analyzed by immunoblotting with anti-p62, anti-LC3, anti-Myc, anti-Flag, anti-HA, and anti-GAPDH. Results are shown for n = 3 independent experiments (representative immunoblotting results are shown).

**c-d. ORF3a from bat-CoV *RaTG* inhibits bat STING dCTT-triggered autophagy induction.** HEK293T cells were co-transfected with Myc-cGAS and *Myd*STING dCTT or *Rss*STING dCTT in the presence or absence of vectors expressing bat *RaTG* ORF3a. Cells were harvested 24 h after transfection. The indicated proteins were

analyzed by immunoblotting with anti-p62, anti-LC3, anti-Myc, anti-Flag, anti-HA, and anti-GAPDH. Results are shown for n = 3 independent experiments (representative immunoblotting results are shown).

**e-f. *Rss*STING dCTT activation suppresses HSV-1 GFP replication, which can be partially restored by ORF3a from bat CoVs.** HEK293T cells were transfected with bat *RaTG* ORF3a or bat *ZC45* ORF3a alone, or co-transfected with Myc-cGAS and *Rss*STING dCTT in the presence or absence of vectors expressing bat *RaTG* ORF3a and bat *ZC45* ORF3a for 20 h, and subsequently infected with HSV-1 GFP for 24 h. GFP-positive cells were analyzed by FACS. The relative HSV-1 GFP positivity is shown in (**f**). Empty vector with HSV-1 GFP infection served as a control and was set to 100%. Statistical significance was determined by two-sided unpaired *t*-test. Means and standard deviations are presented. Results are shown for n = 4 independent experiments.

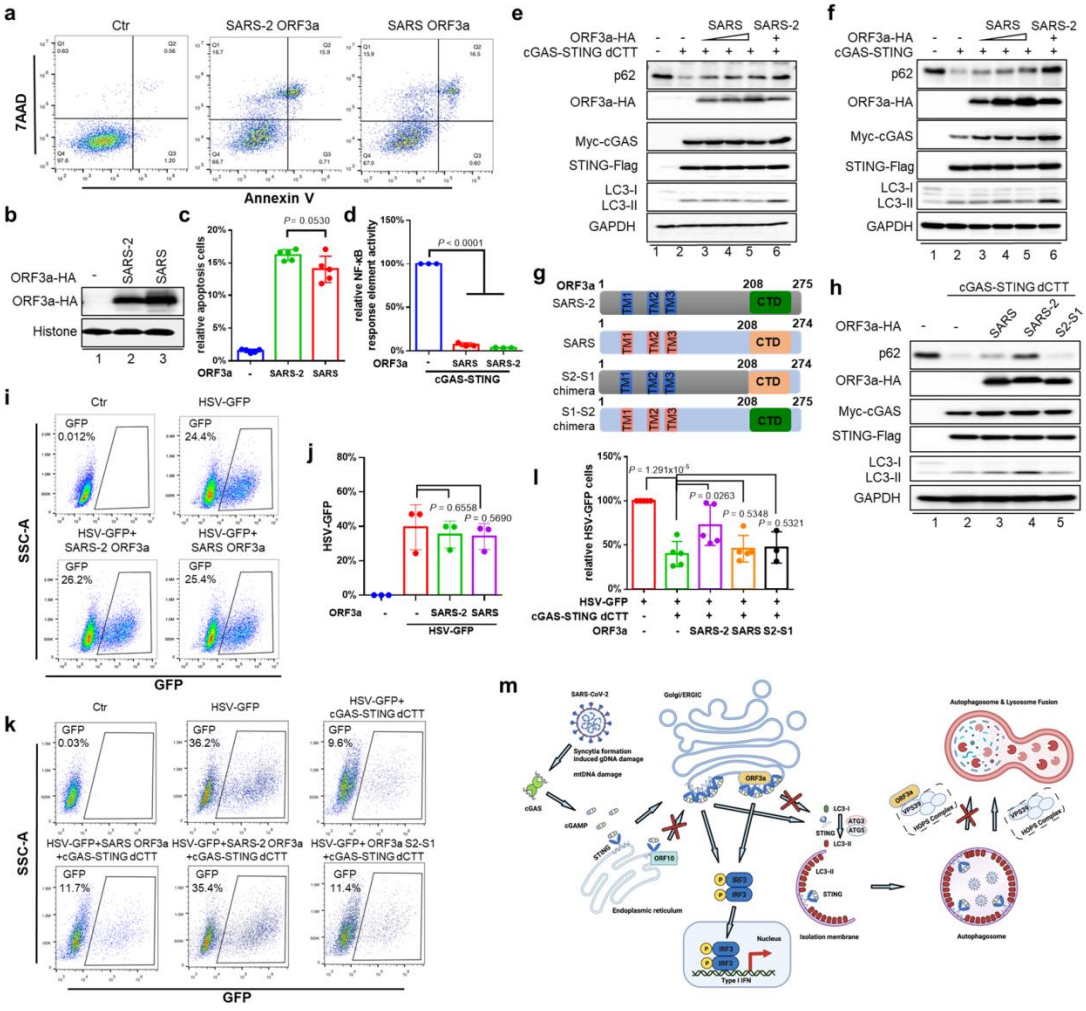


**Fig. 4 SARS-CoV ORF3a is less effective in restraining STING-mediated autophagy than is SARS-CoV-2 ORF3a.**

**a-c. SARS-CoV ORF3a and SARS-CoV-2 ORF3a produce comparable levels of apoptosis induction.** HEK293T cells were transfected with ORF3a from SARS-CoV or SARS-CoV-2. At 24 h after transfection, the cells were stained with Annexin V-APC and 7-AAD for flow cytometry analysis. Results are shown for n = 3 independent

experiments (representative results are shown). The percentage of apoptotic cells in (**a)** was measured (**c**). Statistical significance was determined by two-sided unpaired *t*-test. Means and standard deviations are presented. ORF3a expression was analyzed by immunoblotting with anti-HA. Histone served as an internal control (**b**). Results are shown for n = 5 independent experiments (representative immunoblotting results are shown).

**d. Both SARS-CoV ORF3a and SARS-CoV-2 ORF3a inhibit cGAS-STING-mediated NF-κB activity.** HEK293T cells were co-transfected with NF-κB-Luc, Myc-cGAS, and STING-Flag expression vectors in the presence or absence of SARS-CoV ORF3a and SARS-CoV-2 ORF3a. pRL-TK *Renilla* was used as an internal control. Transactivation of the luciferase reporter was determined 24 h after transfection. cGAS-STING alone served as a control and was set to 100%. Results are shown for n = 3 independent experiments. Means and standard deviations are presented. Statistical significance was determined by two-sided unpaired *t*-test.

**e-f. SARS-CoV ORF3a is deficient in suppressing autophagy induced by STING or STING dCTT activation.** HEK293T cells were co-transfected with Myc-cGAS and STING or STING dCTT expression vectors in the presence or absence of SARS-CoV-2 ORF3a and increasing amounts of SARS-CoV ORF3a. Cells were harvested 24 h after transfection. The indicated proteins were analyzed by immunoblotting with anti-p62, anti-LC3, anti-HA, anti-Myc, anti-Flag, and anti-GAPDH. Results are shown for n = 3 independent experiments (representative immunoblotting results are shown).

**g. Schematic of ORF3a chimeras.**

**h. Chimeric ORF3a S2-S1 cannot suppress cGAS-STING dCTT-induced autophagy.** HEK293T cells were co-transfected with the Myc-cGAS and STING dCTT-Flag expression vectors in the presence or absence of SARS-CoV-2 ORF3a, SARS-CoV ORF3a, and chimeric ORF3a S2-S1. Cells were harvested 24 h after transfection. The indicated proteins were analyzed by immunoblotting with anti-p62, anti-LC3, anti-HA, anti-Myc, anti-Flag, and anti-GAPDH. Results are shown for n = 3 independent experiments (representative immunoblotting results are shown).

**i-j. ORF3a alone from SARS-CoV or SARS-CoV-2 has no effect on HSV-1 GFP replication.** HEK293T cells were transfected with SARS-CoV or SARS-CoV-2 ORF3a alone for 20 h and subsequently infected with HSV-1 GFP for 24 h. GFP-positive cells were analyzed by FACS (**i**). The percentage of GFP-positive cells is shown (**j**). Empty vector served as a control. Statistical significance was determined by two-sided unpaired *t*-test. Means and standard deviations are presented. Results are shown for n = 3 independent experiments.

**k-l. ORF3a from SARS-CoV and the S2-S1 chimera are compromised in their ability to restore HSV-1 GFP replication suppressed by cGAS-STING dCTT when compared to SARS-CoV-2 ORF3a.** HEK293T cells were co-transfected with Myc-cGAS and STING dCTT-Flag in the presence or absence of vectors expressing SARS-CoV-2 ORF3a, SARS-CoV ORF3a, and chimeric ORF3a S2-S1 for 20 h, then infected with HSV-1 GFP for 24 h. GFP-positive cells were analyzed by FACS (**k**). The

relative HSV-1 GFP positivity is shown in (**I**). The empty vector with HSV-1 GFP infection served as a control and was set to 100%. Statistical significance was determined by two-sided unpaired *t*-test. Means and standard deviations are presented. Results are shown for n≥3 independent experiments.

**m. A model representing the mechanism of SARS-CoV-2 ORF3a-mediated suppression of cGAS-STING-autophagy.**